Evaluation of MODIS LST Products Over the Tibetan Plateau and Plain Areas With in Situ Measurements

Yuting Qi, Lei Zhong, Yaoming Ma, Yunfei Fu, Zixin Wang, and Peizhen Li

***Abstract*—Land surface temperature (LST) is a crucial physical parameter for hydrological, meteorological, climatological, and climate change studies. To encourage the use of satellite-derived LST products in a wide range of applications, providing feedback on product performance over regional and global scales is an urgent task. However, considering that the uncertainty of newly released LST products is still unclear, it is urgently necessary to perform a comprehensive validation and error analysis, especially in areas with special geographical and weather conditions, such as the Tibetan plateau (TP). In particular, fewer studies have been concerned with the degraded LST retrieval accuracy over the TP because of the sparse ground measurements. In this study, moderate-resolution imaging spectroradiometer (MODIS) LST products (C6.1) were comprehensively evaluated based on the independent ground observation systems with different atmospheric and LST conditions. The in situ measurements collected from the Tibetan Observation and Research Platform and surface radiation systems are located on the American Plain and the TP, respectively, incorporating various land-cover types, including barren land, grassland, cropland, shrubland, and sparse and dense vegetation, among others. The spatial representativeness evaluation indicated that relatively high-quality in situ LSTs can be obtained during nighttime. Compared with the North American Plain (with a mean RMSE of 1.56 K), MODIS LST retrievals have larger discrepancies (mean RMSE of 2.34 K) over the TP with complex terrain and weather conditions. Emissivity determination is the primary source of the uncertainty in the generalized split-window (GSW) algorithm. Moreover, simulation settings of atmospheric and LST conditions in the GSW algorithm cannot cover a wide range of conditions at a global scale. It is expected to develop new LST retrieval algorithm to meet the quality specifications of users over the TP. Overall, this study identifies critical further research needs and improves the understanding of LST product performance under complex circumstances.**

***Index Terms*—In situ measurements, land surface temperature (LST), moderate-resolution imaging spectroradiometer (MODIS), temperature-based validation method, Tibetan plateau (TP).**

I. Introduction

LAND surface temperature (LST) is one of the indispensable parameters in the study of land surface processes on different scales, combining the results of energy and water cycle between the land surface and above atmosphere [1], [2], [3], [4]. LST has also been widely used in various applications, including land-cover change analysis [5], [6], surface flux estimation [7], [8], climate change research [9], drought monitoring [10], and soil moisture estimation [11]. Meanwhile, LST has also been serving as an environmental climate variable by the global climate observing system [12]. Remote sensing in thermal infrared (TIR) provides a unique method of obtaining LST information at regional and global scales [13], [14], [15], [16]. Many algorithms for LST retrieval have been developed, including the single-channel algorithm [17], the split-window algorithm [13], and the temperature-emissivity separation (TES) algorithm [18], among others. Some LST products have been released using different algorithms, such as the moderate-resolution imaging spectroradiometer (MODIS) LST product, satellite application facility on land surface analysis LST product, and advanced spaceborne thermal emission and reflection radiometer (ASTER) surface kinetic temperature product, among others [1], [5].

NASAs Earth observing system on the terra and aqua platforms is equipped with the MODIS sensor, regarded as one of the critical instruments to provide various and reliable remote sensing products [19]. The most popular algorithm for LST retrieval is the generalized split window (GSW), which provides the LST products at 1-km spatial resolution with a temporal resolution of four times daily (from terra and aqua platforms) in most regions [20]. The GSW algorithm applies a simple form so that it requires less computing time [13]. In recent decades, various refinements have been implemented to pursue high-quality LSTs. In particular, separate sets of coefficients for retrieving over bare soil surfaces were improved in the recently released Collection 6 MODIS LST product [21]. Although product developers have made many improvements, far fewer studies have been undertaken to comprehensively evaluate remotely sensed LSTs globally due to the difficulty of obtaining actual LST data, especially in heterogeneous and

Received 19 March 2024; revised 28 April 2024; accepted 14 August 2024. Date of publication 23 August 2024; date of current version 5 September 2024. This work was supported in part by the Second Tibetan Plateau Scientific Expedition and Research (STEP) program under Grant 2019QZKK0103, in part by the National Natural Science Foundation of China under Grant 42375071, Grant 42425502, Grant 42230610, and Grant 41875031, in part by DTE-CLIMATE in the framework of the ESA–MOST Dragon 6 program under Grant 95357, and in part by the School of Earth and Space Sciences, CMA-USTC Laboratory of Fengyun Remote Sensing, University of Science and Technology of China. *(Corresponding author: Lei Zhong.)*

Yuting Qi, Yunfei Fu, Zixin Wang, and Peizhen Li are with the School of Earth and Space Sciences, CMA-USTC Laboratory of Fengyun Remote Sensing, University of Science and Technology of China, Hefei 230026, China (e-mail: qiyuting@mail.ustc.edu.cn; fyf@ustc.edu.cn; wangzixin@mail.ustc.edu.cn; lipz@mail.ustc.edu.cn).

Lei Zhong is with the School of Earth and Space Sciences, CMA-USTC Laboratory of Fengyun Remote Sensing, University of Science and Technology of China, Hefei 230026, China, and with Jiangsu Collaborative Innovation Center for Climate Change, Nanjing 210023, China, and also with CAS Center for Excellence in Comparative Planetology, Hefei 230026, China (e-mail: zhonglei@ustc.edu.cn).

Yaoming Ma is with the State Key Laboratory of Tibetan Plateau Earth System, Resources and Environment (TPESRE), Institute of Tibetan Plateau Research, Chinese Academy of Sciences, Beijing 100101, China, and also with the College of Earth and Planetary Sciences, University of Chinese Academy of Sciences, Beijing 100049, China (e-mail: ymma@itpcas.ac.cn).

Digital Object Identifier 10.1109/JSTARS.2024.3448355

complex underlying surfaces [e.g., Tibetan plateau (TP)] [22], [23]. Meanwhile, detailed error analysis for evaluating product uncertainty is also urgently needed to provide developers with suggestions for algorithm improvement.

In general, three methods are used for validating LST products: the temperature-based (T-based) method [24], [25], [26], the radiance-based (R-based) method [27], and the intercomparison method [28]. Except for the underlying surface of barren land, previous studies have shown that the quality of the MODIS LST product was better than 1 K at most investigated stations based on the T-based validation method [29]. For instance, Duan et al. [25] validated the refined C6 MODIS LST product based on in situ observations over various underlying, with an RMSE value of more than 2 K during the daytime and less than 2 K during the nighttime. Li et al. [27] evaluated the MODIS LST products over four bare soil surface stations in an arid area of northwest China. The results indicated that there is an obvious underestimation of the MODIS LST products, with biases varying from −0.91 K to −3.76 K. However, according to current validation studies, long-term comprehensive and robust LST product validation was primarily conducted with low altitude and homogeneous surfaces due to more accessible validation data with well-maintained stations [30].

Additionally, the evaluations of remote sensing products lack consistent and sufficient validation results, making it impossible to obtain persuasive and high-quality LSTs globally [31]. In addition, there is still no perfect method for various cases. The R-based method provided an alternative way to evaluate satellite-derived LST products by using radiative transfer simulations in the absence of ground measurements [22]. However, this method cannot be used for heterogeneous or nonisothermal surfaces and generally requires contemporaneous atmospheric profiles and a priori knowledge of LSE. Obviously, the TP cannot meet the conditions because the atmospheric profiles cannot be easily obtained. In addition, the intercomparison validation method is usually used as a supplementary validation while it is difficult to provide quantitative values of accuracy [25]. The most direct and effective method was to directly compare the remote-sensed LST with ground-based measurements. Generally, T-based validation requires the accurate knowledge of surface emissivity and temporally matched longwave radiances of field stations.

In recent decades, great efforts have been made to perform validation studies using different sensors at different scales [32], [33], [34]. The TP is the highest and largest plateau in the world, with complex terrain, variable weather conditions, and heterogeneous surfaces [35]. As aforementioned, poor-quality LST retrieval was reported at the underlying surface of bare soil [24]. While the TP has large areas of barren land, few studies focus on the performance of LST retrieval. Moreover, the degraded LST retrieval accuracy over the TP has also rarely been witnessed and is regarded as one of the obstacles hindering LST application [33], [36]. Therefore, it is crucial to accurately reveal the accuracy of LST products over the TP. However, the observational data are scarce due to the high cost and difficulty of maintaining ground stations over the TP for a long time [36], [37]. After decades of effort, long-term observation networks [such as the Tibetan Observation and Research Platform (TORP)] with optimized scientific designs and layouts have been established. Unprecedented opportunities have been provided for the evaluation and analysis of LST products. In this study, long-term comprehensive evaluations of MODIS LST products were conducted over the TP using the latest TORP dataset. Possible reasons for satellite-derived LST uncertainties were analyzed, and the directions for improving the retrieval algorithm were clarified. In addition, to obtain more persuasive results, validation stations located at the plain were also added for comparison.

The main objectives of this study are to explore the accuracy of the improved C6.1 MODIS LST products under different atmospheric and surface conditions and to analyze the LST retrieval uncertainties and further provide algorithm improvement directions. The rest of this article is organized as follows. A brief description of the study area and data is presented in Section II. Section III provides a detailed description of the methodology for assessment and robust outlier removal methods used in this article. The results of the MODIS LST products evaluation are presented and analyzed in Section IV. The discussion is presented in Section V. Furthermore, Section VI concludes this article.

II. Study Area and Data

A. Study Area

The TP is critical in impacting global atmospheric circulations, producing mechanical and thermal effects on air masses or airflow [35]. Substance and energy transport between the land surface and atmosphere of the TP have a profound impact on local and regional climate. As the highest and largest plateau, the TP has an average elevation of 4000 m [37], [38]. The TP has distinctive landscapes that encompass various underlying surfaces, including vast glacier, snow, permafrost, alpine meadow, grassland, etc. The IPCC Sixth Assessment Report indicates that the global average temperature has risen by 1.1 °C after industrialization, and the TP has shown a faster warming rate of 0.25 °C decade^{-1} [39], [40]. However, due to the TPs harsh environments, a comprehensive understanding of remote-sensed LST products is insufficient, which limits their specific applications [35], [40]. Consequently, the TP was chosen as one of the study areas (see Fig. 1).

Meanwhile, to reveal the different performances of satellite-derived LST products, a supplemental study area is needed to provide helpful information regarding comparative validation. Taking the data quality, accessibility, and geographical location matching into account, the American Plain was selected as the comparative validation area (see Fig. 1). Similar to the geographic location of the TP, the American Plain is located in the Northern Hemisphere with flat terrain and covers diverse atmospheric and surface conditions, including grassland, shrubland, cropland, and meadow, among others [41].

B. Data

1) Ground-Based Measurements: The U.S. surface radiation (SURFRAD) budget network provides long-term and quality-controlled SURFRAD budget measurements over the United States after 1993, which includes seven carefully chosen and well-maintained stations covering diverse climates [26].

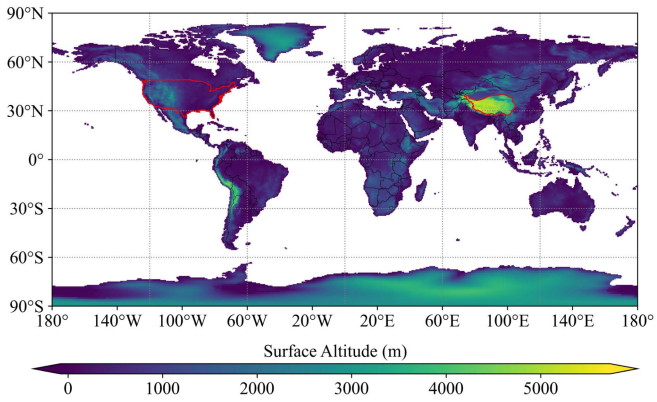

Fig. 1. Geographical location of the study area (red line marks). The left panel is the location of SURFRAD representing the plain region, and the right panel is the location of the TORP representing the plateau region. The color bar shows the altitude.

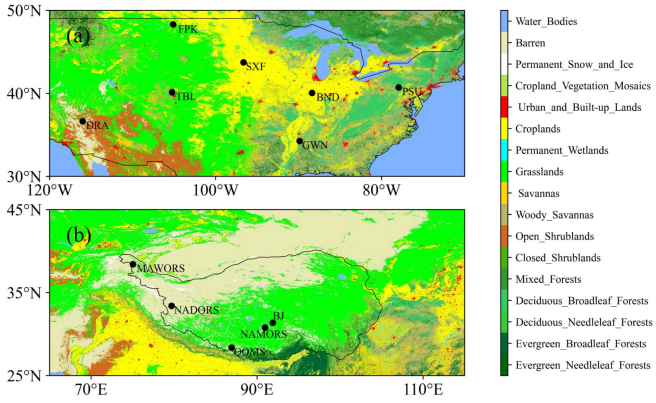

Fig. 2. Locations of the seven SURFRAD and five TORP stations used in this study. The color bar shows the land-cover types of the ground stations, which were obtained from the MCD12Q1 products (defined by IGBP).

Fig. 2 shows the locations and land-cover types of the investigated stations, and Table I provides detailed information. The data can be downloaded from the Global Monitoring Laboratory.[1] All the stations are located in flat agricultural areas covered by crops and grass, except for the DRA site surrounded by open shrublands [see Fig. 2(a)]. The vegetation and landscape around the stations are relatively homogeneous [41]. The land surface emissivity of these stations was consistently high, which was estimated from the ASTER global emissivity dataset based on a linear regression equation [42]

$$\varepsilon_b = 0.197 + 0.025\varepsilon_{10} + 0.057\varepsilon_{11} + 0.237\varepsilon_{12} + 0.333\varepsilon_{13} + 0.146\varepsilon_{14} \quad (1)$$

where ε_{10}–ε_{14} are the bands 10–14 surface emissivities obtained from ASTER GED V3 data, and ε_b is the broadband emissivity of each station. Specifically, the calculated ε_b values are 0.973, 0.968, 0.972, 0.967, 0.971, 0.970, and 0.971 for FPK, DRA, TBL, BND, GCM, PSU, and SXF, respectively.

The SURFRAD network was designed to provide a 1-min observation of each parameter after 2009. SURFRAD instruments are carefully maintained and regularly replaced with freshly calibrated instruments to ensure good observational performance [43]. The data were measured from the Eppley precision infrared radiometer at 10 m height, and the effective diameter of the field-of-view was approximately 70 m [41]. The upwelling and downwelling TIR radiances from Eppley precision infrared radiometer were used to derive ground-based LST, which has an estimated uncertainty of $\pm$3–5 W/m^2 [44]. As reference datasets for long-term LST validation, SURFRAD measurements have been successfully applied to evaluate various satellite-derived LST products [25], [44].

The TORP presents a long-term ground measurement dataset of land–atmosphere interaction observations composed of six field stations (MAWORS, NADORS, QOMS, NAMORS, BJ, and SETORS) distributed in the TP [33]. Note that the SETORS stations were unavailable in this study because of monitoring problems of long-wavelength radiation [35]. The remaining five stations are covered by alpine steppe, desert, and meadow [see Fig. 2(b); Table I]. To show the complex and heterogeneous surface of the TP, the terrain features and land-cover types around the TORP stations were provided in Fig. 3. Land-cover-type data were obtained from finer resolution observation and monitoring global land-cover (FROM-GLC) product, which is the first 30-m resolution global land-cover maps [45]. The MAWORS station is situated in the northwestern TP, surrounded by large-scale glaciers, whose land is predominantly sandy soil. It is worth noting that the standard deviation (STD) of elevation within a kilometer around the MAWORS station is 152.92 m, the highest among the five stations. The NADORS station is in an open valley covered by desert and gravel. The BJ station was built in a flat prairie with high grass density, whose soil type is predominantly silt loam. The NAMORS station is covered with sparse vegetation and is near Nam Co Lake. Finally, the QOMS station lies in the Rongbuk Valley, and the land-cover type is grassland.

The TORP provided observations with 30-min temporal resolution from 2017 to 2020 and an hourly temporal resolution from 2005 to 2016. The T-based validation method involves direct comparison with ground measurements performed at the homogenous stations concurrent with the satellite overpassing time. To reduce errors caused by observation time mismatches between satellite and ground measurements as much as possible, the 2017–2020 data were used for validation. The datasets are available at the Science Data Bank.[2]

A four-component radiation flux observing system (CNR1) from Kipp and Zonen was installed at each station and contained upward and downward pyrgeometers for outgoing and incoming longwave radiation flux with approximately 5% W/m^2 observation uncertainty [33]. The CNR1 was installed at a height of 1.5 m with an FOV of approximately 150°, and the diameter of its detection circular at the surface is approximately 12 m. The TORP observational dataset also provided data that can be used for long-term validation of LST datasets, e.g., MODIS, SLSTR, and Landsat. The LSE acquisition method is the same as the SURFRAD network in this study, and the surface broadband emissivities were 0.963, 0.942, 0.968, 0.944, and 0.949 for MAWORS, NADORS, NAMORS, QOMS, and BJ, respectively.

1.[Online]. Available: https://gml.noaa.gov

2.[Online]. Available: https://doi.org/10.11922/sciencedb.00103

TABLE I
DETAILED INFORMATION ON THE GROUND-BASED MEASUREMENTS USED IN THIS STUDY

Network	Stations	Latitude	Longitude	Elevation	MODIS IGBP land cover type	Land cover type
SURFRAD	BND	40.05°N	88.37°W	230 m	Croplands	Croplands
	SXF	43.73°N	96.62°W	473 m	Croplands	Croplands
	FPK	48.31°N	105.11°W	634 m	Grasslands	Grasslands
	GWN	34.25°N	89.87°W	98 m	Woody_Savannas	Cropland/natural vegetation mosaic
	DRA	36.62°N	116.02°W	1007 m	Barren	Open shrublands
	PSU	40.72°N	77.93°W	376 m	Croplands	Cropland/natural vegetation mosaic
	TBL	40.12°N	105.23°W	1689 m	Grasslands	Grasslands
TORP	QOMS	28.35°N	86.94°E	4298 m	Grasslands	Alpine desert
	MAWORS	38.40°N	75.04°E	3668 m	Grasslands	Alpine desert
	NAMORS	30.76°N	90.97°E	4730 m	Grasslands	Alpine steppe
	NADORS	33.39°N	79.69°E	4270 m	Barren	Alpine desert
	BJ	31.37°N	91.89°E	4509 m	Grasslands	Alpine meadow

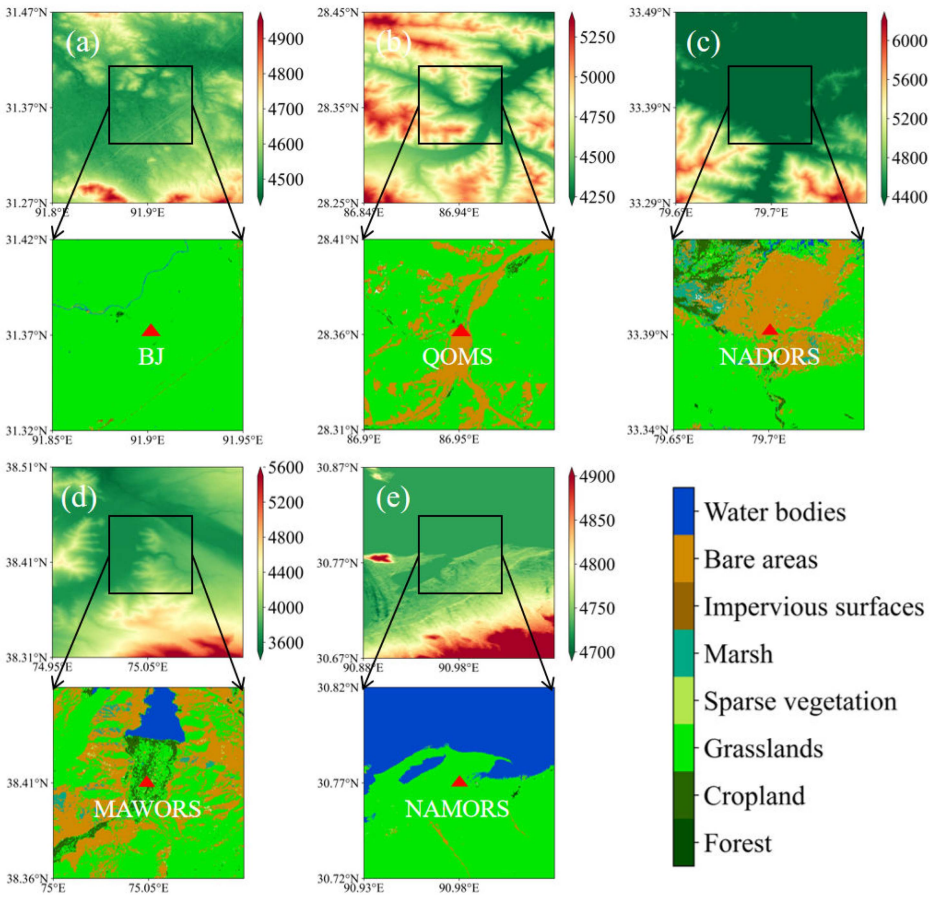

Fig. 3. Terrain features and land-cover types of five TOPR stations (a: BJ, b: QOMS, c: NADORS, d: MAWORS, and e: NAMORS) used in this study. The digital elevation model was from ASTER GDEM product (unit: m), and land-cover-type data were obtained from FROM-GLC product.

2) MODIS LST/Emissivity Products: MODIS instruments were onboard the terra and aqua satellite platforms for global coverage observations. Terra overpasses at local solar times of 10:30 A.M. with the product name prefix "MOD," while Aqua overpasses at approximately local solar times of 1:30 P.M. with the product name prefix "MYD." Note that the M∗D11A1 products with stricter cloud filters were used in this study rather than the M∗D11_L2 products to reduce the cloud contamination effect [46]. The MODIS land surface products (MOD11A1 and MYD11A1) have operationally supplied global coverage of LST and surface emissivity dataset. Meanwhile, new refinements of the GSW algorithm have been introduced to improve its accuracy [47].

For the GSW algorithm, the coefficients depend on the surface air temperature, atmospheric water vapor, and viewing zenith angle according to radiative transfer simulations. Only one set of coefficients was used in the C5 GSW algorithm to retrieve LSTs for each group of underlying types [18]. However, due to the poor accuracy and rapid diurnal variation of LST retrieval in bare soil surfaces, separate sets of coefficients within the latitude range from $-38°$ to 49.5° were set for retrieving LST in the newly released C6.1 products. Meanwhile, the GSW algorithm also improves the LSE estimation, simulation temperature setting range, and relevant formulae. According to the previous sensitivity analysis, the GSW algorithm is more sensitive to the emissivity difference between MODIS bands 31 and 32 than the emissivity mean [19], [47]. Therefore, the algorithm adjusted emissivity differences and kept the corresponding emissivity mean constant for barren land pixels.

In addition, the coefficients in GSW algorithm were obtained by regressing the simulated satellite signal with a set of atmospheres and surface parameters [13]. Radiative transfer simulations need to cover a wide range of atmospheric and LST conditions to ensure retrieval accuracy at global scales. The simulated land surface and atmospheric temperatures are set to 280–325 K for the daytime and 275–305 K for the nighttime. The difference between LSTs and air temperature ranges from 8 to 29 K for daytime LSTs and from -10 to 4 K for nighttime LSTs, while the range is set as ± 16 K for other underlying surfaces during daytime and nighttime. A description of the improved algorithm can be found in [19].

The refined GSW algorithm is expressed as follows:

$$T_s = b_0 + \left(b_1 + b_2\frac{1-\varepsilon}{\varepsilon} + b_3\frac{\Delta\varepsilon}{\varepsilon^2}\right)\frac{T_{31}+T_{32}}{2} + \left(b_4 + b_5\frac{1-\varepsilon}{\varepsilon} + b_6\frac{\Delta\varepsilon}{\varepsilon^2}\right)\frac{T_{31}-T_{32}}{2} + b_7(T_{31}-T_{32})^2 \tag{2}$$

where T_s is the satellite-derived LST, and are the mean and the difference of the emissivities in bands 31 and 32, respectively. The b_i ($i = 0$–6) are the regression coefficients obtained from radiative transfer simulations based on MODTRAN4 [13], [19].

The long-term MODIS LST products (MOD11A1 and MYD11A1) during the period of 2017–2020 were downloaded from the Level-1 and Atmosphere Archive and Distribution System Distributed Active Archive Center.[3] The geographic latitude and longitude data were extracted to ensure the accurate geometric positioning, and the science dataset layer quality control was used to eliminate cloud contamination for the LST and LSE datasets.

3) Auxiliary Data: To further analyze the error source, auxiliary data were introduced in this study, mainly involving remote sensing, ground-based, and reanalysis datasets (see Table II).

The ASTER sensor was launched in 1999 and acquired by sensors on NASA satellite platforms, with a wavelength domain range between 8 and 12 μm [18]. The ASTER global emissivity dataset (ASTER GED V3) is a static product (mean emissivity from 2000 to 2008) with 90 m spatial resolution. Hulley et al. [48] indicated that the ASTER GED product has higher retrieval accuracy over most land-cover types. Therefore, the ASTER GED V3 product was frequently used as a reference to evaluate the quality of emissivity products. Because of the different spectral response functions between ASTER and MODIS, it is necessary to convert the corresponding ASTER emissivity values to MODIS [28]. Based on the spectral response function of two sensors and the ASTER spectral library, the ASTER GED V3 product was converted into emissivity values corresponding to MODIS bands 31 and 32 by a linear regression equation [25], [28]. In addition, ASTER TIR data were also used to generate the surface kinetic temperature products (AST_08) at 90-m and 1-km spatial resolutions [48], [49]. The AST_08 data were used to evaluate the spatial representativeness and describe the spatial variability of land surface biophysical parameters around the investigated stations in this study [28].

Additional remote sensing products were the MODIS level-2 atmospheric profile product at 5-km spatial resolution (MOD07_L2 and MYD07_L2) and the MODIS land-cover-type product (MCDLC1KM) at 1-km spatial resolution [20]. The atmospheric water vapor content (ACWV) generated from M∗D07_L2 products requires high accuracy as a crucial input variable in the GSW algorithm. Meanwhile, the MCDLC1KM product was the primary reference to determine the surface emissivity. As the input data to generate MODIS LST, it is urgently necessary to pay attention to its accuracy.

In addition, the Japan International Cooperation Agency China–Japan climate disaster mitigation project (JICA/Tibet project) was downloaded to validate column water vapor data over the TP [4]. A total of six radiosonde sites were extracted after quality control. Finally, ERA5-land provides hourly land variables with 0.1° spatial resolution over several decades [50]. In this study, the 2 m air temperature and skin temperature were collected to obtain the differences in land surface and atmospheric conditions for two study areas.

III. Methodology

A. Temperature-Based Validation Method

In this article, T-based validation method was conducted for MODIS LST products based on TORP and SURFRAD observation networks. Only the high-quality data were evaluated based on minimizing the cloud contamination effect on the evaluation results [51]. Satellite-derived LST and ground-based LST were temporally and spatially matched. The in situ LST estimation method and its uncertainty are presented in the following content.

3.[Online]. Available: https://doi.org/10.11922/sciencedb.00103

TABLE II
DATASET INFORMATION USED IN THIS STUDY

Dataset	Products	Temporal and Spatial resolution	Variables	Download URL
Remote sensing data	MOD11 & MYD11	1 km /Twice a day	LSE, LST	https://ladsweb.modaps.eosdis.nasa.gov/
	MOD07 & MYD07	5 km /Twice a day	WVC	
	MCDLC1KM	1 km /Twice a day	LCT	
	ASTER GED	90 m	LSE	https://search.earthdata.nasa.gov/
	ASTER LST	90 m/16 day	LST	
Reanalysis data	ERA5-land	100 km / Hourly	Tair, LST	https://cds.climate.copernicus.eu/
In situ measurement	TORP	30 min	Longwave radiation	https://doi.org/10.11922/sciencedb.00103
	SURFRAD	1 min	Longwave radiation	
	JICA	Hourly	Radiosonde	https://data.tpdc.ac.cn/zh-hans/data/d8f184da-f87d-4455-a034-7622e6cc89f2

1) In Situ LST Estimation: Both the pyrgeometers installed in the SURFRAD stations and the CNR1 net radiometers at the TORP stations provided hemispherical longwave radiances [25], [35]. In situ LST was estimated from the measured downwelling and upwelling radiances according to Stefan Boltzmann's law [52]

$$\mathrm{LST}_{\mathrm{insitu}} = \left[\frac{\mathrm{UL} - (1-\varepsilon_b)\,\mathrm{DL}}{\sigma\varepsilon_b}\right]^{1/4} \tag{3}$$

where $\mathrm{LST}_{\mathrm{insitu}}$ is the estimated measured LST (K) of each station, UL is the upward longwave radiation ($\mathrm{W/m^2}$), DL is the downward longwave radiation ($\mathrm{W/m^2}$), σ is the Stefan–Boltzmann constant (5.67×10^{-8} $\mathrm{W/m^2/K^4}$), and $\varepsilon_b$is the broadband emissivity for each station.

2) In Situ LST Uncertainty: Although the in situ LST is easy to obtain from radiometers or pyrgeometers, the uncertainty of $\mathrm{LST}_{\mathrm{insitu}}$ calculated by (3) for each station was crucial for the T-based validation. High quality in situ LSTs are often challenging to obtain because of various influencing factors. There are four main factors that affect the accuracy of in situ LSTs, including emissivity uncertainty, radiometer observation error, temporal mismatch, and spatial heterogeneity [44].

Specifically, the LSE input for calculating the in situ LST data has an emissivity uncertainty of ±0.01, equivalent to an LST error range of ±0.3 K to ±0.5 K (σ_{emis}) [49]. Meanwhile, the longwave radiation pyrgeometers equipped by the SURFRAD network and the CNR1 net radiometers from the TORP have an estimated uncertainty (σ_{cal}) of $\pm$ 5 $\mathrm{W/m^2}$, which will result in an LST uncertainty of approximately 0.3 K [23]. Meanwhile, the adjacent time data from ground stations were extracted to match the satellite overpass time. However, the TORP system only provided observations with a 30-min temporal resolution, while the SURFRAD network temporal resolution was 1 minute. The relatively low temporal resolution will cause a relatively large error for calculating in situ LST. In this study, the land surface diurnal temperature cycle of each station was extracted to calculate the uncertainty caused by LST temporal variability. The results indicated that the uncertainty for the SURFRAD network was smaller than 0.25 K, while the uncertainty of the TORP observation system is relatively large (with a mean bias up to 0.48 K). Another crucial influencing factor is the spatial representativeness of the ground measurements. The AST08 product has been successfully used to assess the spatial representativeness of in situ LST due to its high spatial resolution (90 m at nadir). In this study, all available AST08 clear-sky data corresponding to MODIS LST products were downloaded. A subset of 11×11 ASTER LST pixels and simultaneous MODIS LST pixels was used to calculate the average value of the spatial STD (σ_{spat}).

Therefore, the total uncertainty of each station was provided by a combination of the four error sources as follows:

$$\sigma_{\mathrm{LST}} = \left[\sigma_{\mathrm{emis}}{}^2 + \sigma_{\mathrm{cal}}{}^2 + \sigma_{\mathrm{temp}}{}^2 + \sigma_{\mathrm{spat}}{}^2\right]^{1/2}. \tag{4}$$

B. Robust Outlier Removal

The SURFRAD network applies the standards for the measurement set developed by the baseline SURFRAD network, which can provide the accurate data that meet world standards [43]. Special consideration was given to the stations distributed over the TP, which must apply strict data quality control to detect problematic data due to the harsh environments, highly complex terrains, and heterogeneous underlying surfaces [35]. In addition, the MODIS cloud mask product (MOD35 and MYD35) was adopted to identify clear-sky scenes used in LST retrieval. However, the accuracy of LST retrieval was greatly affected by the misclassification of cloudy pixels as clear sky, especially for neighboring cloudy pixels [2]. Therefore, quality control is needed for TORP observation data and MODIS LST products before validation. The anomaly detection toolkit (ADTK) Python package was adopted for outlier detection in this study.

The ADTK package is an unsupervised machine learning model that offers a set of common outlier detectors, transformers, and aggregators with unified APIs and pipe classes that connect them into models [53]. The combination of different

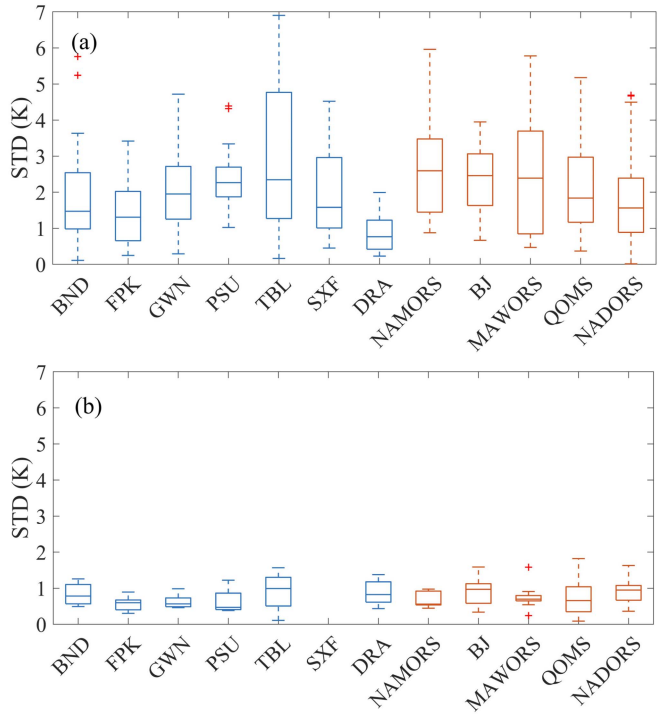

Fig. 4. Comparison between ASTER LST products (a subset of 11×11 pixels) and corresponding MODIS LST products for (a) daytime and (b) nighttime. The red plus signs indicate the outliers.

modules can effectively respond to different types of data. For the station observation data, the applied ADTK package first processes the time-series features based on the transformer module and then detects anomalies based on the mutation point detection method. Compared with the popular three-edit rule method, this method is more suitable for detecting outliers in continuous time-series data, especially for field data [25].

IV. Results and Analyses

A. Spatial Representativeness Evaluation and Uncertainty of Ground-Measured LST

By comparing LST images of different resolutions, the relative thermal homogeneity for each station was assessed. In this study, the ASTER LST product with 90-m spatial resolution and the corresponding MODIS LST product with 1-km spatial resolution were used to evaluate the spatial representativeness of the TORP and SURFRAD stations. Specifically, a subset of 11×11 ASTER LST pixels and corresponding MODIS LST pixels were used to calculate the spatial STD of LST during daytime and nighttime. A median STD less than 1 K is considered homogeneous, according to Guillevic et al. [23].

Fig. 4 presents the comprehensive comparison results in the form of boxplots. The results indicated that LST exhibits higher spatial heterogeneity during the daytime than at night. Meanwhile, the average STD of TP stations is slightly higher than that of SURFRAD stations, which means relatively high heterogeneity of plateau stations can be identified compared with plain stations. All of the investigated stations during nighttime can be selected for evaluation, while only a few stations during daytime meet the requirements. This is due to that the air temperature is closer to the surface temperature at night, and the spatial thermal environment is more homogeneous [3]. Using only LST products during nighttime can effectively reduce errors caused by spatial variations in LST.

Furthermore, there are relatively small errors for the SURFRAD observation network located in the plain, with total uncertainties less than 1 K. The ground-based LST uncertainties are greater than 1 K over the TORP stations, with values of 1.05, 1.12, and 1.01 K obtained for the MAWORS, BJ, and NAMORS stations. Therefore, the evaluation accuracy of these stations is acceptable with a reasonable range.

B. Validation of the MODIS LST Products

The C6.1 MODIS LST products derived from the GSW algorithm were validated by the TORP and SURFRAD stations during nighttime from 2017 to 2020. Fig. 5 shows MODIS LST versus in situ LST at seven SURFRAD stations under relatively homogeneous thermal conditions. The evaluation results demonstrated that the MODIS LST products were generally consistent with ground-measured LSTs over plain stations. The RMSE was little than 2 K at all SURFRAD stations except for the DRA station. Negative biases were obtained for MODIS LST products over most investigated stations, while slight positive biases were identified at GWN and PSU station. In addition, the accuracy of the MYD11 (aqua) product is slightly higher than that of MOD11 (terra) over the SURFRAD station (see Table III). However, for the DRA station, there is an obvious underestimation of the LST product with an RMSE up to 4.59 K. Meanwhile, similar systematic errors were also reported in VIIRS LST products when directly compared with in situ measurements [54]. According to Duan et al. [25], the larger uncertainty may be attributed to viewing geometry differences between in situ radiometer and satellite sensor. Specifically, in situ radiometers view more bushes (close to air temperature) than the directional satellite over the DRA stations during nighttime. Overall, except for the DRA station, MODIS LST products have satisfactory performance at SURFRAD stations located in plain areas, with a mean RMSE of 1.56 K.

In contrast, relatively large uncertainty for MODIS LST products can be found over the TP (see Fig. 6). The land-cover types over the TP at the satellite pixel scale were grouped into three categories:

1) barren land surface (QOMS, MAWORS, and NADORS);
2) grassland (BJ);
3) savannas with sparse vegetation coverage (NAMORS).

The evaluation results show that there is a significant difference in LST retrieval performance at the three bare soil stations, with an RMSE of 1.56 K, 2.05 K, and 3.06 K for QOMS, NADORS, and MAWORS, respectively. Meanwhile, the retrieval performance gradually degraded as the LST increased at MAWORS station. For the NAMORS and BJ stations with vegetation cover, the evaluation results were larger than 2 K, with an RMSE of 2.63 K and 2.69 K, respectively. Furthermore, negative biases of the C6.1 MODIS LST product were obtained for all investigated stations over the TP. Similarly, the accuracy of the MYD11 products is higher than that of MOD11, especially in terms of the NAMORS station (see Table III). Generally,

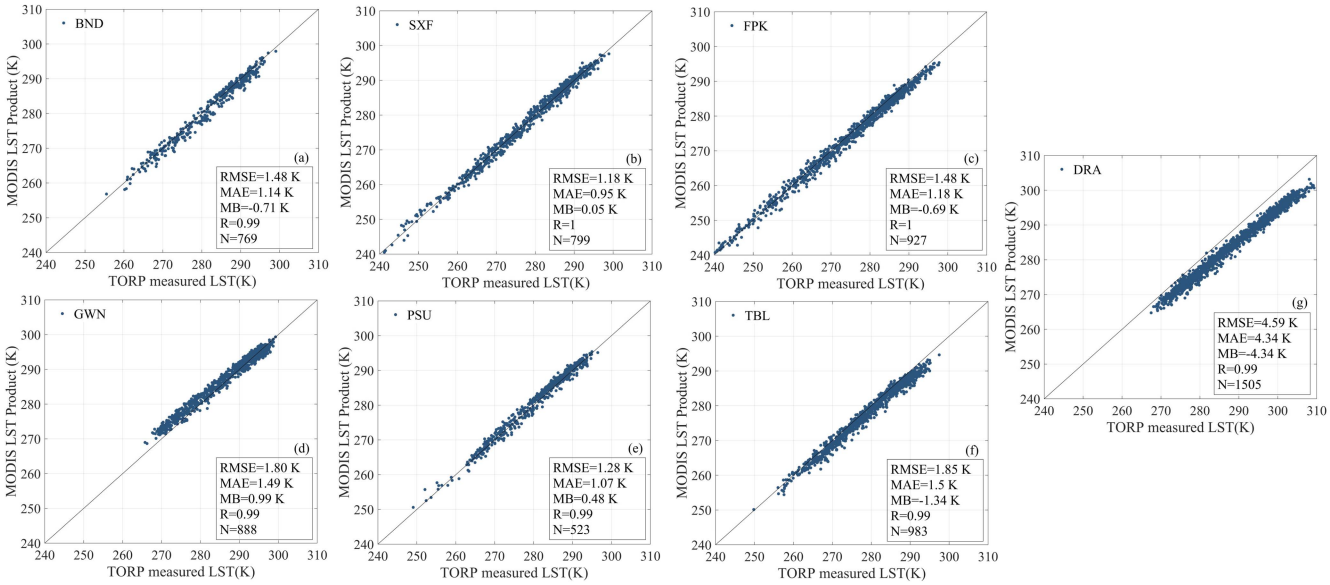

Fig. 5. Scatterplots of C6.1 MODIS LST products (MOD11 and MYD11) against in situ LSTs during nighttime at SURFRAD stations. (a) BND. (b) SXF. (c) FPK. (d) GWN. (e) PSU. (f) TBL. (g) DRA.

TABLE III
STATISTICAL INDICATORS FOR THE COMPARISON BETWEEN C6.1 MODIS LST AND GROUND-BASED LST AT NIGHTTIME

Network	Stations	MOD11 (TERRA)			MYD11 (AQUA)		
		Num	Bias (K)	RMSE (K)	Num	Bias (K)	RMSE (K)
SURFRAD	BND	392	-0.69	1.37	377	-0.74	1.51
	GWN	471	0.99	1.82	417	0.98	1.79
	PSU	261	0.46	1.29	262	0.51	1.27
	SXF	386	-0.26	1.24	413	-0.95	1.10
	FPK	501	-0.67	1.59	426	-0.71	1.39
	TBL	479	-1.45	1.94	504	-1.21	1.73
	DRA	803	-4.59	4.65	702	-4.11	4.53
TORP	QOMS	637	-1.07	1.76	473	-0.64	1.23
	MAWORS	664	-2.68	3.31	543	-1.92	2.71
	NAMORS	347	-1.17	3.16	337	-0.45	1.94
	NADORS	942	-1.03	1.72	724	0.62	1.81
	BJ	516	-0.93	2.89	577	-0.79	2.48

substantial discrepancies exist in satellite LST retrieval over the TP, with a mean RMSE of 2.34 K.

C. Refined Analysis of Validation Results

The reasons for the uncertainties of satellite-derived LST over the TP need to be clarified by further analysis. The coefficients in the GSW algorithm were derived from regression analysis of a set of simulation datasets based on MODTRAN code, which is crucial for LST retrieval from TIR remote sensing data. In this process, there are various factors that affect the LST retrieval accuracy, such as classification-based surface emissivity estimation, ACWV, and satellite observation geometry, among others. In the following, a dedicated analysis was conducted on the simulation condition settings, input data error accumulation, and other factors.

1) Simulation Settings of Atmospheric and LST Conditions: Prior to the analysis for each station, the general atmospheric and

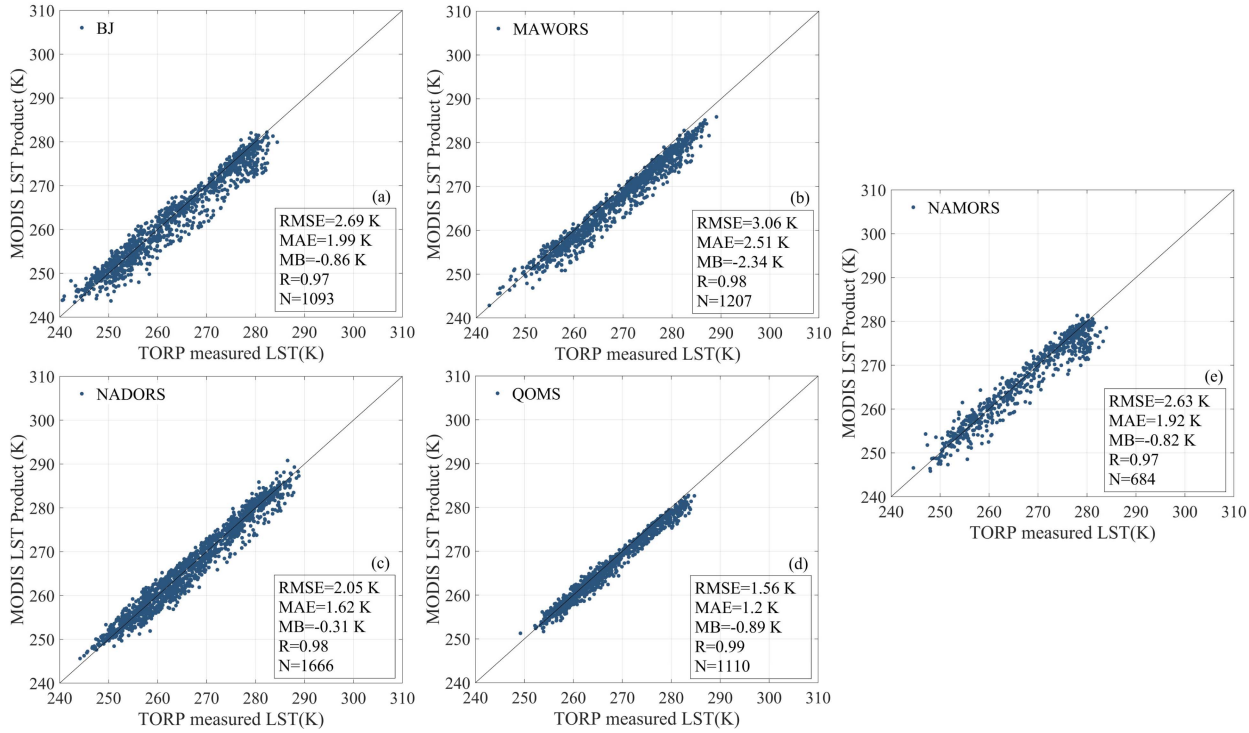

Fig. 6. Scatterplots of C6.1 MODIS LST products (MOD11 and MYD11) against in situ LSTs during nighttime at TORP stations, (a) BJ, (b) MAWORS, (c) NADORS, (d) QOMS, and (e) NAMORS.

LST conditions in the study areas were explored. According to the above-mentioned results, separate sets of algorithm coefficients in the bare soil zone and other surfaces were obtained by different simulation conditions. Although the daytime LST data were not validated due to insufficient spatial representativeness, the data covering all satellite overpass periods were calculated to present the actual conditions of the two study areas. Based on the above considerations, statistics were conducted on atmospheric and LST conditions, and corresponding underlying surfaces were distinguished.

Atmospheric and LST conditions were acquired from the ERA-5 land dataset during 2020. The results indicated that the environmental discrepancy in the two study areas was obvious, with lower and wider ranges of air temperature and LST over the TP (see Fig. 7). It is attributed to the high altitudes, variable weather conditions, and complex terrain of the TP. Because of the wide range of bare soil LSTs in different seasons, the bare soil was extracted and compared with other underlying surfaces (see Fig. 7). Specifically, there are obvious discrepancies in LST conditions between the plateau and plain, with relatively lower LST at nighttime and higher LST at daytime over the plateau [see Fig. 7(a) and (b)]. Especially for the barren land, the relatively larger differences in LST conditions can be identified. In addition, the LST may often exceed 325 K during daytime or below 265 K during nighttime at the plateau.

Those conditions may be beyond the simulation setting range in the GSW algorithm. For the air temperature condition over the two areas, a frequency distribution similar to LST conditions can be observed over all underlying surface types [see Fig. 7(c)–(d)]. However, unlike LST, there is a relatively small discrepancy over the barren underlying area between the plain and plateau. Overall, to avoid the LST uncertainties induced by simulation settings, significant discrepancies between plateau and plain environments should be considered. To pursue higher accuracy over challenging area, such as the TP, it is necessary to introduce more simulated datasets in GSW algorithm to cover wider ranges of atmospheric and surface conditions.

Meanwhile, according to the GSW algorithm settings, the range of (LST-T_{air}) is set from 8 to 29 K for daytime LST and from -10 to 4 K for nighttime LST over barren land within latitude range from $-38°$ to 49.5°, varying from -16 to $+16$ K for other land surface types [19]. Obviously, the actual LST-T_{air} condition may exceed the simulation setting range over the plateau (see Fig. 8). In most cases, the condition set by the algorithm better matches the actual situation in plain areas. However, the errors in the LST retrieval may be larger in plateaus where the absolute value of LST-T_{air} is larger than the setting range.

2) Uncertainty of Land Surface Emissivity and Water Vapor Content: Radiances measured from satellite radiometers were greatly affected by LSE [20]. In the MODIS GSW algorithm, the LSE in both TIR channels is known as a priori [28]. Meanwhile, atmospheric quantities were approximately parameterized as a function of the AWVC to solve the ill-posed problem [13]. Therefore, it is also necessary to focus on the accuracy of LSE and AWVC. Due to the MODIS LST product providing poorer accuracies over the plateau than that of plain area, two key variables of LSE and AWVC were collected to further analyze the error sources.

According to different land-cover types, emissivity values can be estimated by classification method based on MODIS

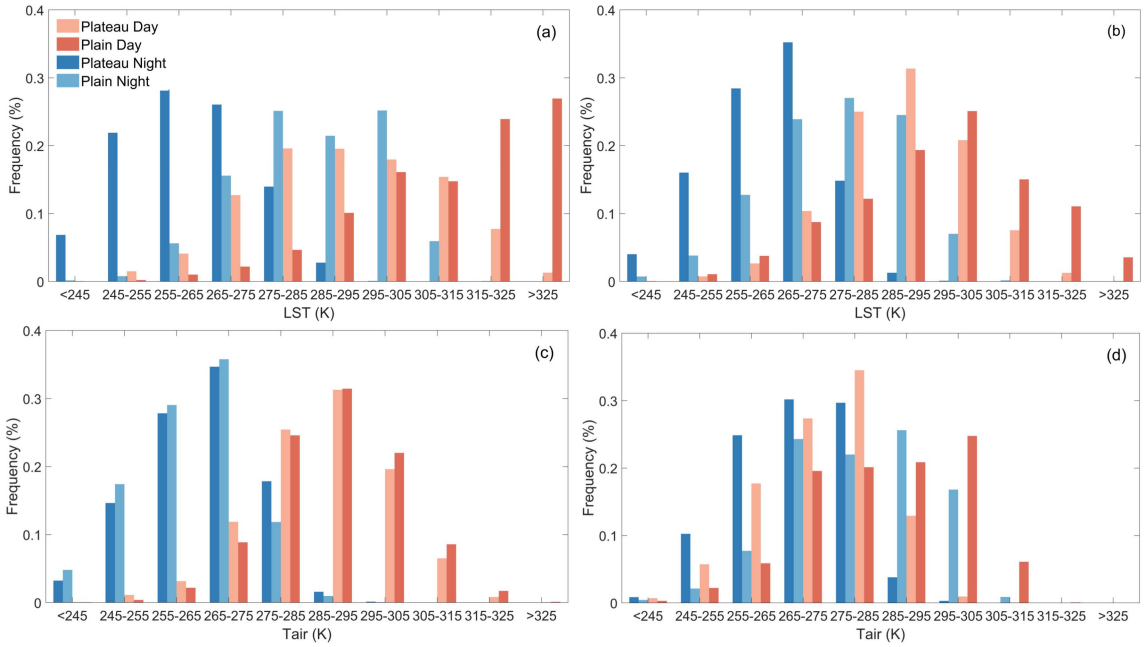

Fig. 7. Annual surface and atmospheric conditions of different land-cover types in the plateau and plain areas obtained from the ERA-5 land dataset. The surface temperature conditions of (a) barren land and (b) other underlying surface types, and the air temperature conditions of (c) barren land and (d) other underlying surface types.

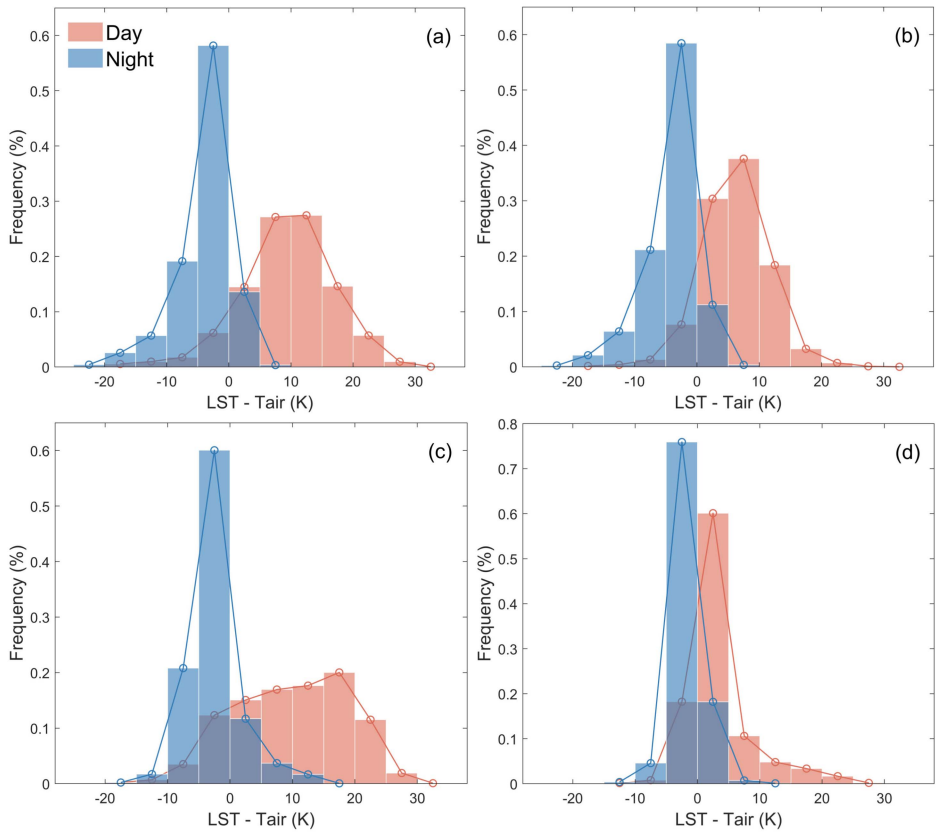

Fig. 8. Frequency histogram of LST minus air temperature during daytime and nighttime. Statistical values over the (a) plateau barren land, (b) plateau other underlying surface types, (c) plain barren land, and (d) plain other underlying surface types.

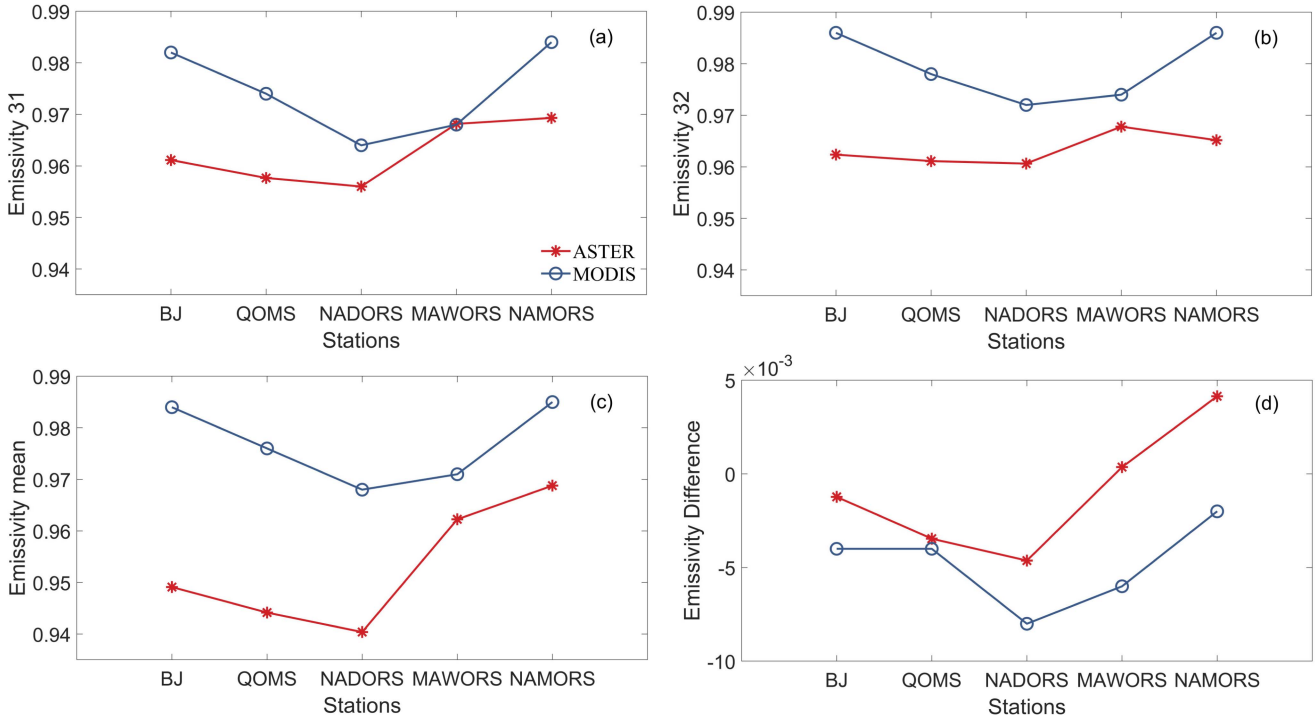

Fig. 9. Comparison of C6.1 MODIS emissivity products (MxD11) with ASTER GED V3 data at TORP stations.

land-cover-type product [25]. Specifically, the mean and difference MODIS emissivity values (bands 31 and 32) were compared with the converted ASTER GED V3 at the TORP stations (see Fig. 9). It should be noted that there is no significant difference in surface emissivity (bands 31 and 32) between the terra MOD11 and aqua MYD11 products [55]. Therefore, the average values of MOD11 and MYD11 LSE products were used for comparison with the ASTER GED V3 products. According to the previous sensitivity analysis, the retrieval algorithm is more sensitive to the emissivity difference ($\Delta\varepsilon$) values than the emissivity mean [13], [14]. In terms of the QOMS station, $\Delta\varepsilon$ is more accurate than mean emissivity, which may be the reason for the highest accuracy of LST retrieval among the five stations. For the BJ station, the surface type was correctly classified as grasslands, and $\Delta\varepsilon$ value is close to ASTER GED V3 data. However, the mean emissivity has a large discrepancy for the BJ station. This is likely due to the ASTER GED V3 data providing a static LSE product from 2000 to 2008, which could be unable to capture the annual and interannual variability in LSE for this station. For the MAWORS and NAMORS stations, misclassification of surface types leads to emissivity errors. Meanwhile, fixed values assigned by the accurate classification do not necessarily represent the natural and dynamic emissivity at 1-km spatial resolution, especially over barren land, such as the NADORS station. The land-cover type of this station is equivalently correct, while significant error can be found in $\Delta\varepsilon$ values. Meanwhile, the spatial distribution of LSE from ASTER GED V3 and MODIS over the TP was provided for comparison (see Fig. 10). Obviously, the MODIS LSE products are overestimated. Note that the overestimated emissivity will cause an underestimation of LST according to Li et al. [44]. An

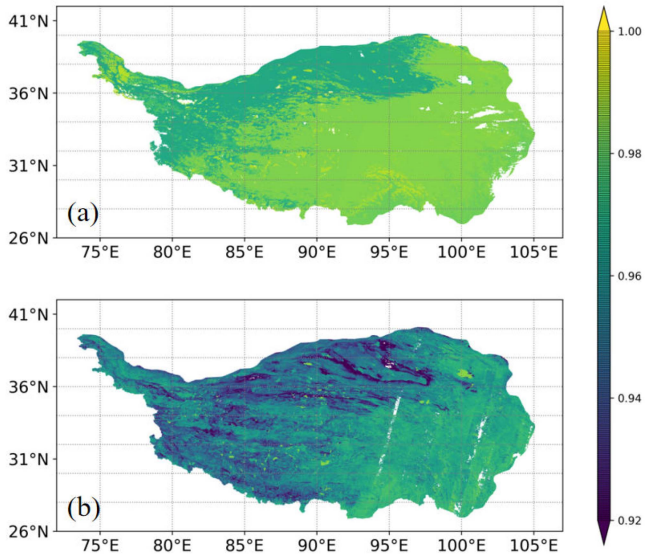

Fig. 10. Spatial distribution of annual average broadband LSE over the TP. (a) MODIS LSE product (MxD11). (b) ASTER GED V3.

LSE estimation error of approximately 0.01 will cause an error ranging from 0.3 to 0.5 K for LST retrieval [5], [49]. Based on the LSE analyses, it can be found that spectral emissivity uncertainty was the main uncertainty source for the MODIS LST product over the TP.

Another error source that has rarely received attention is the uncertainty of AWVC over the TP. In terms of MODIS data,

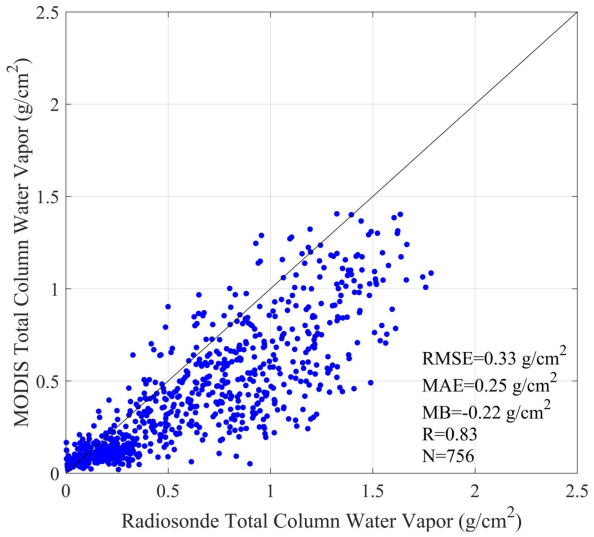

Fig. 11. Scatterplot of the comparison between the radiosonde and satellite-derived atmospheric water vapor.

the AWVC data were collected from the MODIS level-2 atmospheric profile product, which consists of several temperature and moisture profile parameters. Unfortunately, owing to the TPs high altitude, dynamic climates, and harsh environmental conditions, it is difficult to measure the relative humidity profile at an accuracy better than 10% [1], [56]. By comparing the AWVC data generated from M∗D07_L2 products with radiosonde total column water vapor over six stations, valuable information regarding AWVC discrepancies was obtained (see Fig. 11). Theoretically, the AWVC uncertainty should be less than 0.3 g/cm^2 [22]. It is obvious that the RMSE of AWVC is large and concentrated in cases with high water vapor content. The LST retrieval accuracy will degrade under a highly humid atmosphere in the GSW algorithm. Therefore, the inaccuracy of AWVC estimation can cause significant errors in LST retrieval. Meanwhile, in the simulation process, the AWVC has a wider range, which varies from nearly 0 to 5.5 cm. However, atmospheric conditions beyond this range may frequently occur over the TP, especially for water vapor transfer channels. Consequently, the accurate ACWV estimation over the TP is a key focus in future studies.

3) Other Factors: Except for the relatively large uncertainty caused by the simulation process and input data, there is a long-standing issue that the brightness temperature observed by the sensor is anisotropic. For instance, the LST disparities viewing from different geometry directions may range from −2 to 5 K, especially for the TP with highly complex terrain [32]. To analyze the angular effect of remotely sensed LST, data with satellite zenith angles (SZAs) greater than 45° were removed. Removing data with larger observation angles slightly improved accuracy for all investigated stations. The stations with considerable error (larger than 2 K) were greatly influenced by the angle effect (see Table IV). Among them, the LST retrieval accuracy at MAWORS station is significantly affected by larger SZAs, with an accuracy improvement of up to 0.42 K. This is attributed to the high terrain complexity and heterogeneity around the MAWORS station [35]. In addition, the NAMORS and BJ stations also

TABLE IV
COMPARISON OF VALIDATION RESULTS BEFORE AND AFTER REMOVING LARGER SZAS AT THE MAWORS, BJ, AND NAMORS STATIONS

Stations	Before remove		After remove	
	Num	RMSE (K)	Num	RMSE (K)
MAWORS	1207	3.05	870	2.63
NAMORS	684	2.63	478	2.31
BJ	1093	2.69	808	2.40

have corresponding improvements in accuracy. In general, the degradation of retrieval accuracy under a larger view zenith angle is an urgent problem that restricts comparisons between different products.

Meanwhile, errors may be introduced by limitations of validation methods. It is extremely difficult to obtain field LSTs with high-quality spatial representativeness. Meanwhile, limited by high altitude, harsh environment, and maintenance costs, only one radiation instrument was generally equipped at each station. Therefore, detailed information about the LST spatial distribution around the station cannot be obtained. In this study, the relatively homogenous LST spatial distribution around each investigated station was confirmed by using LST images with high spatial resolutions. In addition, a total uncertainty of in situ LST for each station was also provided as a reference. However, it is impossible to ensure that each satellite pixel is homogenous. To further explore the impact of LST variations at the satellite scale, only the MODIS LST products with an STD less than 1 K were evaluated. The result indicated that relatively high accuracy can be obtained for all stations (see Fig. 12). Note that the temporal resolution of the ASTER sensor is low, which greatly reduces the number of available validations.

In addition, to analyze the bias variability, the monthly mean bias was calculated over the TORP station, as shown in Fig. 13. There is no significant difference in monthly mean bias for MODIS LST product during nighttime, except for the BJ station. The monthly mean bias of BJ station ranges from −3.30 to −1.34 K, with a smaller uncertainty during summer. This is probably due to the increasing maturity of underlying vegetation providing a more homogeneous and isothermal distribution around this station during this period. Therefore, the evaluation results will also be affected by variations in vegetation biophysical conditions around the station.

V. DISCUSSION

A. Uncertainties of the MODIS LST and Emissivity Product Over the TP

In situ measurements from two study areas were utilized to comprehensively evaluate the MODIS LST product accuracy. According to the analyses above, the accuracy of LST retrieval over the TP was influenced by various factors, including simulation settings of atmospheric and LST conditions, the LSE and AWVC estimation, and angular anisotropy.

The coefficients of the GSW algorithm were regressed from rigorous radiative transfer simulations, and the simulated database can only cover most of the conditions [19]. Based

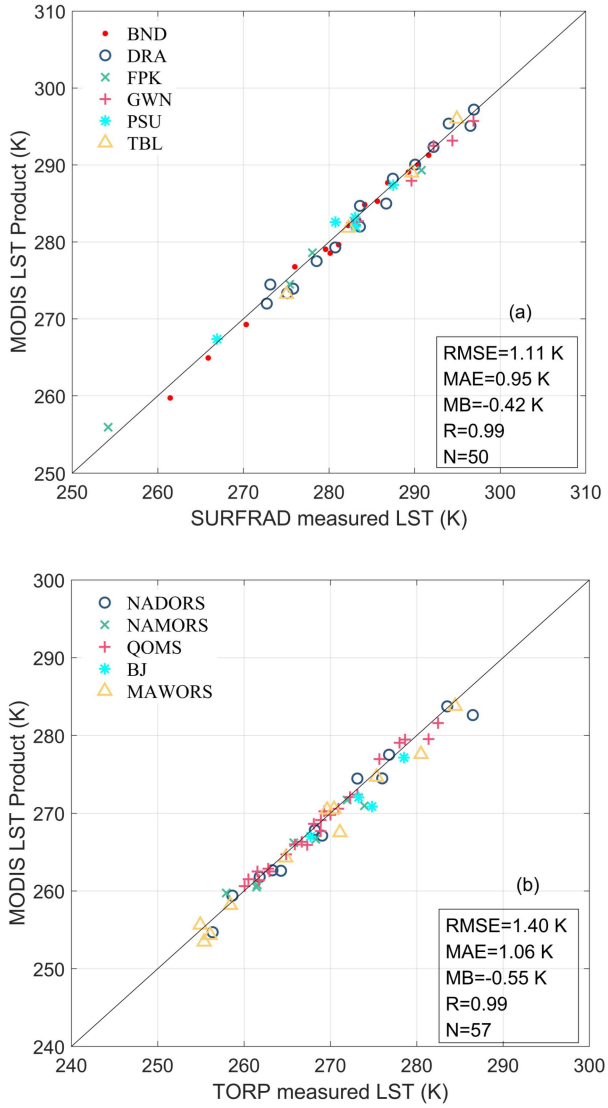

Fig. 12. Validation results by in situ LST with high-quality spatial representativeness at (a) SURFRAD stations and (b) TORP stations.

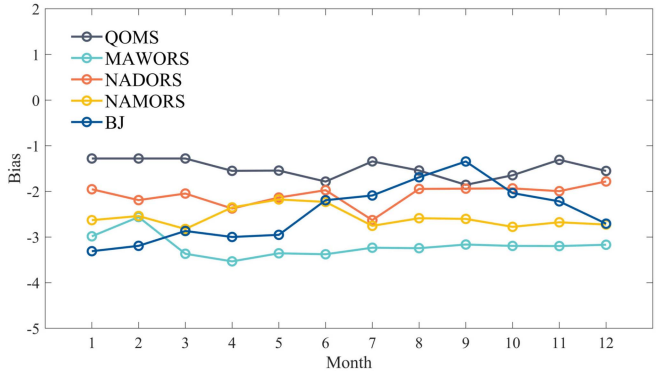

Fig. 13. Statistical results of monthly mean bias (remote-sensed LST minus in situ LST) at nighttime from 2017 to 2020.

TABLE V
STATISTICAL DATA FOR THE PROPORTION OF UNDERLYING SURFACE TYPES FROM DIFFERENT PRODUCTS OVER THE TP

LCT_Type	GLC_FCS30D	CGLS	MCD12Q1
Forest	10.40%	9.31%	5.08%
Cropland	1.25%	0.75%	0.03%
Grassland	59.67%	43.24%	54.48%
Impervious surfaces	0.32%	0.10%	0.06%
Bare / sparse vegetation	23.82%	42.56%	37.39%
Water body	2.46%	1.95%	1.33%
Permanent ice and snow	2.10%	2.03%	1.39%

Land-cover classification data for comparison were provided by the Copernicus global land service (CGLS) product at a resolution of 100 m and the GLC_FCS30D product at a resolution of 30 m [45], [59].

on the considerations of the unique environment of the TP, it is challenging to collect datasets from various stations under different atmospheric and surface conditions. Therefore, improving algorithms by separating them into several tractable subranges, especially in the TP with unique climates, is an effective and appropriate method [5].

The main error source of LST retrieval over the TP is the error propagation of input data (LSE and AWVC). Based on the classification-based emissivity method, the LSE was assigned according to the land-cover-type product. This process did not accurately represent the seasonal variation in emissivity [56]. Hulley et al. [48] compared the ASTER GED and MODIS LSE products based on a spectral library. The results indicated that, without considering seasonal variations, the MODIS LSE will introduce errors in LST retrieval. Moreover, misclassifications can also lead to considerable errors, and LSEs calculated based on the fixed values of a limited number of spectral libraries only partially represent real conditions. Göttsche and Hulley [58] reported that misclassification often occurs in MODIS land-cover-type products. Accordingly, statistical data on the proportion of underlying surface types in different products across the TP are provided in Table V. The results indicated that there are significant differences in the classification of different land-cover types of products [45], [56], [59]. In particular, for the classification of grasslands and bare soil (such as the QOMS and MAWORS stations), the two types exhibit different spectral characteristics in the TIR band. Consequently, the accuracy of emissivity data should be improved over the TP.

Meanwhile, another LST product (MxD21) was further validated for comparison (see Table VI). The results show that there are slight differences in accuracy between these LST products. However, according to Li et al. [27], LSE data obtained from the MOD21 product show good agreement with actual surface characteristics. For the MxD21 products, LSE and LST were simultaneously estimated based on the TES algorithm after accurate atmospheric corrections. In the LST retrieval process, any residual errors in the atmospheric correction may introduce

TABLE VI
STATISTICAL INDICATORS FOR THE COMPARISON BETWEEN TWO LST PRODUCTS (MXD11 AND MXD21) AND GROUND-BASED LST AT NIGHTTIME

Network	Stations	MxD11		MxD21	
		Bias (K)	RMSE (K)	Bias (K)	RMSE (K)
SURFRAD	BND	-0.71	1.48	-0.91	1.52
	GWN	0.99	1.80	0.95	1.67
	PSU	0.48	1.28	0.61	1.48
	SXF	-0.05	1.18	-0.10	1.09
	FPK	-0.69	1.48	-0.52	1.37
	TBL	-1.34	1.85	-1.43	1.92
	DRA	-4.34	4.59	-4.15	4.46
TORP	QOMS	-0.89	1.56	-0.75	1.71
	MAWORS	-2.34	3.06	-2.61	3.42
	NAMORS	-0.82	2.63	-0.92	2.82
	NADORS	-0.31	2.05	-0.22	2.01
	BJ	-0.86	2.69	-0.84	2.43

some errors. Therefore, there are effective methods for introducing dynamic emissivity products (such as the MxD21 product) into the GSW algorithm or performing emissivity adjustment considering land surface changes over heterogeneous land-cover types.

The other key aspect is the accuracy of the MODIS atmospheric profile, which is also a priori knowledge. Comprehensive validations of atmospheric profiles on global scales are usually challenging because of the lack of consistent reference data. Theoretically, only the shape of atmospheric water vapor profile is required instead of absolute values based on the simplification of radiative transfer simulations. The bias of LST retrieval can reach up to 2 K under a highly humid atmosphere for the GSW algorithm [57]. In the special case of the TP, harsh environments and frequent extreme weather events can also make it more difficult. Consequently, it is expected to develop an alternative algorithm to improve the accuracy of atmospheric profile.

Furthermore, the directional brightness temperature resulting in inconsistent observation angles under complex heterogeneous surfaces has attracted widespread attention [25]. Natural land surface at a satellite pixel usually consists of several homogeneous components with different temperatures [27], [57]. Angular anisotropy would degrade the accuracy of LST retrieval, especially in the TP with complex and heterogeneous surfaces. As pointed out by Cao et al. [57], angular anisotropy would lead to different radiation transmittance paths in each observation, when LST variation can reach up to 15 K. Therefore, it is essential to conduct angular effect correction on the satellite-derived LST, namely, normalizing LSTs observed at different angles to the value at the nadir.

B. Challenges of T-Based Validation

Independent and comprehensive assessment is a vitally important process to evaluate LST product accuracies, in which T-based validation is the most straightforward and effective method. According to the previous research, T-based validation is much more effective for homogeneous land surfaces, such as inland water, snow, and cropland [29]. Meanwhile, directly comparing satellite-derived LST with concurrent in situ LST may be problematic as LST spatial distributions may vary up to 10 K at a small scale [27]. Especially for the TP with complex terrain and heterogeneous underlying surfaces, the evaluation of satellite-derived products would be greatly affected by the insufficient spatial representativeness of in situ LST.

To avoid introducing errors as much as possible, the validation process was only performed during nighttime in this study. During this period, the LST spatial distribution is similar to air temperature at satellite pixel scales. Similar results were obtained by exploring the LST spatial distribution from the ASTER sensor with high spatial resolution. Meanwhile, the total uncertainty of ground-based LST for each station was also provided as a reference value for evaluation. Under well-chosen cases, the accuracy of LST retrieval will be improved when the STD is less than 1 K. However, the available number of high-quality in situ LST observations for validation is limited. Therefore, the error introduction is unavoidable in general. In addition, TIR field radiometers are often equipped at a certain height, and such observations will also be affected by vegetation growth dynamics. As noted by Duan et al. [60], an alternate approach can collect high-quality LSTs by establishing multiple field radiometers within a satellite pixel. However, there are few available stations on the TP, which limit T-based validation and make it impossible to operate globally.

Furthermore, even if the spatial distribution of the LST is homogeneous at satellite pixel scale, different observation geometries generated by ground instruments and satellite sensors and the atmospheric influence on ground instruments also degrade the comparability of LST during validation. In fact, the hemispheric temperature collected from ground-based measurements is lower than the temperature from vertical observations [61]. However, it is difficult to correct the directional brightness temperature from satellite sensors because of the wide swaths. Additionally, according to Ma et al. [61], the atmospheric influence in near-surface space can cause in situ LSTs to be overestimated by up to 3.11 K during nighttime [61]. Therefore, further studies should focus on enhancing the accuracy of in situ LSTs.

Many efforts have been made to accurately evaluate remotely sensed products [1], [5]. The T-based method used in this study is a conventional validation method for LST products. Meanwhile, the intercomparison and R-based validation methods frequently serve as supplementary strategies in the absence of in situ LST. Note that the different levels of information about the LST retrieval accuracies can be obtained from those three validation methods. For instance, Gomis-Cebolla et al. [62] obtained different results using three validation methods to present a comprehensive assessment of LST uncertainty. Therefore, quantitative and comprehensive evaluation of satellite-derived products over global scales is still challenging, especially for TP with complex terrain and heterogeneous underlying surfaces [63], [64]. Alternative methods are still expected to be developed for

better validation under heterogeneous or nonisothermal surface conditions.

VI. Conclusion

To evaluate the C6.1 MODIS LST product, T-based validation was performed based on the TOPR and SURFRAD networks. Additionally, the error sources for LST retrieval uncertainties over the TP were also revealed by comprehensive error analysis. The main conclusions are listed as follows.

1) Strict data quality control must be applied to detect problematic data from the stations distributed over the TP due to the harsh environments, highly complex terrains, and heterogeneous underlying surfaces. Moreover, the accuracy of LST retrieval was also affected by the misclassification of cloudy pixels as clear sky. Therefore, a robust outlier detection method based on a machine learning model was applied to flag abnormal values before validation.
2) Owing to the relatively high spatial thermal homogeneity, in situ LSTs obtained from both TORP and SURFRAD stations can be used to evaluate remote-sensed LST products during nighttime.
3) Except for the DRA stations, satellite-derived LST products showed good agreement with the in situ LST over the SURFRAD stations, with a mean RMSE of 1.56 K. However, the MODIS LST products have generally substantial discrepancies over the TP, with a mean RMSE of 2.34 K.
4) The GSW algorithm of MxD11 LST products should be implemented with refinements to improve its accuracy over the TP. Specifically, simulation settings of atmospheric and LST conditions cannot cover a wide range of conditions at global scale. Meanwhile, comprehensive error analysis shows that the systematic bias of LSE and AWVC will cause certain errors in LST retrieval. Among them, inaccurate LSE estimation is the main source causing the LST uncertainties over the TP. Moreover, evidence shows that the angular anisotropy of satellite observation will reduce the LST retrieval accuracy, especially for the TP with complex terrain and heterogeneous underlying surfaces.
5) Furthermore, the evaluation was also affected by the T-based validation method. The limitations of T-based validation methods are related to the in situ LST uncertainties and heterogeneous underlying surfaces at the selected station. For the TP with high spatial heterogeneity, the total uncertainty of in situ LST was greater than that of plain areas.

Acknowledgment

The Authors would like thank to the anonymous reviewers for their helpful comments and suggestions that have significantly improved this article.

References

[1] Z. L. Li et al., "Satellite-derived land surface temperature: Current status and perspectives," *Remote Sens. Environ.*, vol. 131, pp. 14–37, Apr. 2013, doi: 10.1016/j.rse.2012.12.008.

[2] F. M. Göttsche, F. S. Olesen, and A. Bork-Unkelbach, "Validation of land surface temperature derived from MSG/SEVIRI with in situ measurements at Gobabeb, Namibia," *Int. J. Remote Sens.*, vol. 34, no. 9/10, pp. 3069–3083, May 2013, doi: 10.1080/01431161.2012.716539.

[3] S. B. Duan, Z. L. Li, B. H. Tang, H. Wu, and R. L. Tang, "Generation of a time-consistent land surface temperature product from MODIS data," *Remote Sens. Environ.*, vol. 140, pp. 339–349, Jan. 2014, doi: 10.1016/j.rse.2013.09.003.

[4] X. Wang, L. Zhong, and Y. M. Ma, "Estimation of 30 m land surface temperatures over the entire Tibetan plateau based on Landsat-7 ETM+ data and machine learning methods," *Int. J. Digit. Earth*, vol. 15, no. 1, pp. 1038–1055, Dec. 2022, doi: 10.1080/17538947.2022.2088873.

[5] Z.-L. Li et al., "Satellite remote sensing of global land surface temperature: Definition, methods, products, and applications," *Rev. Geophys.*, vol. 61, no. 1, Mar. 2023, Art. no. e2022RG000777, doi: 10.1029/2022rg000777.

[6] N. Utsumi, S. Seto, S. Kanae, E. E. Maeda, and T. Oki, "Does higher surface temperature intensify extreme precipitation?," *Geophysical Res. Lett.*, vol. 38, no. 16, Aug. 2011, Art. no. L16708, doi: 10.1029/2011gl048426.

[7] N. Ge et al., "Estimations of land surface characteristic parameters and turbulent heat fluxes over the Tibetan plateau based on FY-4A/AGRI data," *Adv. Atmos. Sci.*, vol. 38, no. 8, pp. 1299–1314, Aug. 2021, doi: 10.1007/s00376-020-0169-5.

[8] T. R. Xu et al., "Mapping regional turbulent heat fluxes via variational assimilation of land surface temperature data from polar orbiting satellites," *Remote Sens. Environ.*, vol. 221, pp. 444–461, Feb. 2019, doi: 10.1016/j.rse.2018.11.023.

[9] D. X. Tran, F. Pla, P. Latorre-Carmona, S. W. Myint, M. Caetano, and H. V. Kieu, "Characterizing the relationship between land use land cover change and land surface temperature," *ISPRS J. Photogramm. Remote Sens.*, vol. 124, pp. 119–132, 2017, doi: 10.1016/j.isprsjprs.2017.01.001.

[10] W. Zhao, F. P. Wen, Q. M. Wang, N. Sanchez, and M. Piles, "Seamless downscaling of the ESA CCI soil moisture data at the daily scale with MODIS land products," *J. Hydrol.*, vol. 603, Dec. 2021, Art. no. 126930, doi: 10.1016/j.jhydrol.2021.126930.

[11] B. Gallego-Elvira, H. M. Taylor, P. P. Harris, and D. Ghent, "Evaluation of regional-scale soil moisture-surface flux dynamics in Earth system models based on satellite observations of land surface temperature," *Geophysical Res. Lett.*, vol. 46, no. 10, pp. 5480–5488, May 2019, doi: 10.1029/2019gl082962.

[12] R. Hollmann et al., "The ESA climate change initiative satellite data records for essential climate variables," *Bull. Amer. Meteorol. Soc.*, vol. 94, no. 10, pp. 1541–1552, Oct. 2013, doi: 10.1175/bams-d-11-00254.1.

[13] Z. Wan and J. Dozier, "A generalized split-window algorithm for retrieving land-surface temperature from space," *IEEE Trans. Geosci. Remote Sens.*, vol. 34, no. 4, pp. 892–905, Jul. 1996, doi: 10.1109/36.508406.

[14] Z. Wan and Z. L. Li, "A physics-based algorithm for retrieving land-surface emissivity and temperature from EOS/MODIS data," *IEEE Trans. Geosci. Remote Sens.*, vol. 35, no. 4, pp. 980–996, Jul. 1997, doi: 10.1109/36.602541.

[15] J. C. Jiménez-Muñoz and J. A. Sobrino, "A generalized single-channel method for retrieving land surface temperature from remote sensing data," *J. Geophysical Res., Atmos.*, vol. 108, no. D22, Nov. 2003, Art. no. 4688, doi: 10.1029/2003jd003480.

[16] S. Zhou and J. Cheng, "An improved temperature and emissivity separation algorithm for the advanced Himawari imager," *IEEE Trans. Geosci. Remote Sens.*, vol. 58, no. 10, pp. 7105–7124, Oct. 2020, doi: 10.1109/tgrs.2020.2979846.

[17] J. C. Jiménez-Muñoz, J. Cristóbal, J. A. Sobrino, G. Sória, M. Ninyerola, and X. Pons, "Revision of the single-channel algorithm for land surface temperature retrieval from Landsat thermal-infrared data," *IEEE Trans. Geosci. Remote Sens.*, vol. 47, no. 1, pp. 339–349, Jan. 2009, doi: 10.1109/tgrs.2008.2007125.

[18] C. Coll et al., "Temperature and emissivity separation from ASTER data for low spectral contrast surfaces," *Remote Sens. Environ.*, vol. 110, no. 2, pp. 162–175, Sep. 2007, doi: 10.1016/j.rse.2007.02.008.

[19] Z. M. Wan, "New refinements and validation of the collection-6 MODIS land-surface temperature/emissivity product," *Remote Sens. Environ.*, vol. 140, pp. 36–45, Jan. 2014, doi: 10.1016/j.rse.2013.08.027.

[20] Z. M. Wan, "New refinements and validation of the MODIS land-surface temperature/emissivity products," *Remote Sens. Environ.*, vol. 112, no. 1, pp. 59–74, Jan. 2008, doi: 10.1016/j.rse.2006.06.026.

[21] S. B. Duan, Z. L. Li, H. Wu, P. Leng, M. F. Gao, and C. G. Wang, "Radiance-based validation of land surface temperature products derived from collection 6 MODIS thermal infrared data," *Int. J. Appl. Earth Observ. Geoinf.*, vol. 70, pp. 84–92, Aug. 2018, doi: 10.1016/j.jag.2018.04.006.

[22] C. Coll, Z. M. Wan, and J. M. Galve, "Temperature-based and radiance-based validations of the V5 MODIS land surface temperature product," *J. Geophysical Res., Atmos.*, vol. 114, Oct. 2009, Art. no. D20102, doi: 10.1029/2009jd012038.

[23] P. C. Guillevic et al., "Validation of land surface temperature products derived from the visible infrared imaging radiometer suite (VIIRS) using ground-based and heritage satellite measurements," *Remote Sens. Environ.*, vol. 154, pp. 19–37, Nov. 2014, doi: 10.1016/j.rse.2014.08.013.

[24] X. Y. Ouyang, D. M. Chen, S. B. Duan, Y. H. Lei, Y. J. Dou, and G. C. Hu, "Validation and analysis of long-term AATSR land surface temperature product in the Heihe river basin, China," *Remote Sens.*, vol. 9, no. 2, Feb. 2017, Art. no. 152, doi: 10.3390/rs9020152.

[25] S. B. Duan et al., "Validation of collection 6 MODIS land surface temperature product using in situ measurements," *Remote Sens. Environ.*, vol. 225, pp. 16–29, May 2019, doi: 10.1016/j.rse.2019.02.020.

[26] C. Coll et al., "Ground measurements for the validation of land surface temperatures derived from AATSR and MODIS data," *Remote Sens. Environ.*, vol. 97, no. 3, pp. 288–300, Aug. 2005, doi: 10.1016/j.rse.2005.05.007.

[27] H. Li et al., "Temperature-based and radiance-based validation of the collection 6 MYD11 and MYD21 land surface temperature products over barren surfaces in northwestern China," *IEEE Trans. Geosci. Remote Sens.*, vol. 59, no. 2, pp. 1794–1807, Feb. 2021, doi: 10.1109/tgrs.2020.2998945.

[28] S.-B. Duan, Z.-L. Li, J. Cheng, and P. Leng, "Cross-satellite comparison of operational land surface temperature products derived from MODIS and ASTER data over bare soil surfaces," *ISPRS J. Photogramm. Remote Sens.*, vol. 126, pp. 1–10, Apr. 2017, doi: 10.1016/j.isprsjprs.2017.02.003.

[29] C. M. Frey, C. Kuenzer, and S. Dech, "Assessment of mono- and split-window approaches for time series processing of LST from AVHRRA TIMELINE round robin," *Remote Sens.*, vol. 9, no. 1, Jan. 2017, Art. no. 72, doi: 10.3390/rs9010072.

[30] A. Sekertekin and S. Bonafoni, "Land surface temperature retrieval from Landsat 5, 7, and 8 over rural areas: Assessment of different retrieval algorithms and emissivity models and toolbox implementation," *Remote Sens.*, vol. 12, no. 2, Jan. 2020, Art. no. 294, doi: 10.3390/rs12020294.

[31] I. F. Trigo, S. L. Ermida, J. P. A. Martins, C. M. Gouveia, F. M. Göttsche, and S. C. Freitas, "Validation and consistency assessment of land surface temperature from geostationary and polar orbit platforms: SEVIRI/MSG and AVHRR/Metop," *ISPRS J. Photogramm. Remote Sens.*, vol. 175, pp. 282–297, May 2021, doi: 10.1016/j.isprsjprs.2021.03.013.

[32] C. Coll, J. M. Galve, R. Niclòs, E. Valor, and M. J. Barberà, "Angular variations of brightness surface temperatures derived from dual-view measurements of the advanced along-track scanning radiometer using a new single band atmospheric correction method," *Remote Sens. Environ.*, vol. 223, pp. 274–290, Mar. 2019, doi: 10.1016/j.rse.2019.01.021.

[33] Y. Qi, L. Zhong, Y. Ma, Y. Fu, X. Wang, and P. Li, "Estimation of land surface temperature over the Tibetan plateau based on sentinel-3 SLSTR data," *IEEE J. Sel. Topics Appl. Earth Observ. Remote Sens.*, vol. 16, pp. 4180–4194, Apr. 2023, doi: 10.1109/jstars.2023.3268326.

[34] K. C. Wang and S. L. Liang, "Evaluation of ASTER and MODIS land surface temperature and emissivity products using long-term surface longwave radiation observations at SURFRAD sites," *Remote Sens. Environ.*, vol. 113, no. 7, pp. 1556–1565, Jul. 2009, doi: 10.1016/j.rse.2009.03.009.

[35] Y. M. Ma et al., "A long-term (2005-2016) dataset of hourly integrated land-atmosphere interaction observations on the Tibetan plateau," *Earth Syst. Sci. Data*, vol. 12, no. 4, pp. 2937–2957, Nov. 2020, doi: 10.5194/essd-12-2937-2020.

[36] X. D. Liu and B. D. Chen, "Climatic warming in the Tibetan plateau during recent decades," *Int. J. Climatol.*, vol. 20, no. 14, pp. 1729–1742, Nov. 2000, doi: 10.1002/1097-0088(20001130)20:14<1729::Aid-joc556>3.0.Co;2-y.

[37] L. Zhong et al., "Estimation of downwelling shortwave and longwave radiation in the Tibetan plateau under all-sky conditions," *J. Geophysical Res., Atmos.*, vol. 124, no. 21, pp. 11086–11102, Nov. 2019, doi: 10.1029/2019jd030763.

[38] M. A. Yaoming, Y. A. O. Tandong, and W. Jiemin, "Experimental study of energy and water cycle in Tibetan plateau—The progress introduction on the study of GAME/Tibet and CAMP/Tibet," *Plateau Meteorol.*, vol. 25, no. 2, pp. 344–351, 2006.

[39] Y. R. Wang, D. O. Hessen, B. H. Samset, and F. Stordal, "Evaluating global and regional land warming trends in the past decades with both MODIS and ERA5-land land surface temperature data," *Remote Sens. Environ.*, vol. 280, Oct. 2022, Art. no. 113181, doi: 10.1016/j.rse.2022.113181.

[40] A. M. Duan and Z. X. Xiao, "Does the climate warming hiatus exist over the Tibetan plateau?," *Sci. Rep.*, vol. 5, Sep. 2015, Art. no. 13711, doi: 10.1038/srep13711.

[41] J. A. Augustine, J. J. DeLuisi, and C. N. Long, "SURFRAD—A national surface radiation budget network for atmospheric research," *Bull. Amer. Meteorol. Soc.*, vol. 81, no. 10, pp. 2341–2357, Oct. 2000, doi: 10.1175/1520-0477(2000)081<2341:Sansrb>2.3.Co;2.

[42] J. Cheng, S. Liang, Y. Yao, and X. Zhang, "Estimating the optimal broadband emissivity spectral range for calculating surface longwave net radiation," *IEEE Geosci. Remote Sens. Lett.*, vol. 10, no. 2, pp. 401–405, Mar. 2013, doi: 10.1109/lgrs.2012.2206367.

[43] Y. Yu et al., "Validation of GOES-R satellite land surface temperature algorithm using SURFRAD ground measurements and statistical estimates of error properties," *IEEE Trans. Geosci. Remote Sens.*, vol. 50, no. 3, pp. 704–713, Mar. 2012, doi: 10.1109/tgrs.2011.2162338.

[44] H. Li et al., "Evaluation of the VIIRS and MODIS LST products in an arid area of Northwest China," *Remote Sens. Environ.*, vol. 142, pp. 111–121, Feb. 2014, doi: 10.1016/j.rse.2013.11.014.

[45] P. Gong et al., "Finer resolution observation and monitoring of global land cover: First mapping results with Landsat TM and ETM+ data," *Int. J. Remote Sens.*, vol. 34, no. 7, pp. 2607–2654, 2013.

[46] J. Mallick, A. A. Bindajam, S. AlQadhi, M. Ahmed, H. T. Hang, and N. V. Thanh, "A comparison of four land surface temperature retrieval method using TERRA-ASTER satellite images in the semi-arid region of Saudi Arabia," *Geocarto Int.*, vol. 37, no. 6, pp. 1757–1781, Mar. 2022, doi: 10.1080/10106049.2020.1790675.

[47] Z. Wan, Y. Zhang, Q. Zhang, and Z. L. Li, "Quality assessment and validation of the MODIS global land surface temperature," *Int. J. Remote Sens.*, vol. 25, no. 1, pp. 261–274, Jan. 2004, doi: 10.1080/0143116031000116417.

[48] G. C. Hulley, S. J. Hook, E. Abbott, N. Malakar, T. Islam, and M. Abrams, "The ASTER global emissivity dataset (ASTER GED): Mapping Earth's emissivity at 100 meter spatial scale," *Geophysical Res. Lett.*, vol. 42, no. 19, pp. 7966–7976, Oct. 2015, doi: 10.1002/2015gl065564.

[49] G. C. Hulley, C. G. Hughes, and S. J. Hook, "Quantifying uncertainties in land surface temperature and emissivity retrievals from ASTER and MODIS thermal infrared data," *J. Geophysical Res., Atmos.*, vol. 117, Dec. 2012, Art. no. D23113, doi: 10.1029/2012jd018506.

[50] J. Muñoz-Sabater et al., "ERA5-Land: A state-of-the-art global reanalysis dataset for land applications," *Earth Syst. Sci. Data*, vol. 13, no. 9, pp. 4349–4383, Sep. 2021, doi: 10.5194/essd-13-4349-2021.

[51] W. P. Yu, M. G. Ma, H. Yang, J. L. Tan, and X. L. Li, "Supplement of the radiance-based method to validate satellite-derived land surface temperature products over heterogeneous land surfaces," *Remote Sens. Environ.*, vol. 230, Sep. 2019, Art. no. 111188, doi: 10.1016/j.rse.2019.05.007.

[52] V. García-Santos, E. Valor, V. Caselles, M. Mira, J. M. Galve, and C. Coll, "Evaluation of different methods to retrieve the hemispherical downwelling irradiance in the thermal infrared region for field measurements," *IEEE Trans. Geosci. Remote Sens.*, vol. 51, no. 4, pp. 2155–2165, Apr. 2013, doi: 10.1109/tgrs.2012.2209891.

[53] M. Ahmed and I. Neamtiu, "DeAnomalyzer: Improving determinism and consistency in anomaly detection implementations," in *Proc. IEEE Int. Conf. Artif. Intell. Testing*, 2023, pp. 17–25.

[54] D. J. Ghent, G. K. Corlett, F. M. Göttsche, and J. J. Remedios, "Global land surface temperature from the along-track scanning radiometers," *J. Geophysical Res., Atmos.*, vol. 122, no. 22, pp. 12167–12193, Nov. 2017, doi: 10.1002/2017jd027161.

[55] S.-B. Duan and Z.-L. Li, "Intercomparison of operational land surface temperature products derived from MSG-SEVIRI and terra/aqua-MODIS data," *IEEE J. Sel. Topics Appl. Earth Observ. Remote Sens.*, vol. 8, no. 8, pp. 4163–4170, Aug. 2015, doi: 10.1109/jstars.2015.2441096.

[56] S. C. Freitas, I. F. Trigo, J. M. Bioucas-Dias, and F.-M. Göttsche, "Quantifying the uncertainty of land surface temperature retrievals from SEVIRI/Meteosat," *IEEE Trans. Geosci. Remote Sens.*, vol. 48, no. 1, pp. 523–534, Jan. 2010, doi: 10.1109/tgrs.2009.2027697.

[57] B. Cao et al., "A review of Earth surface thermal radiation directionality observing and modeling: Historical development, current status and perspectives," *Remote Sens. Environ.*, vol. 232, Oct. 2019, Art. no. 111304, doi: 10.1016/j.rse.2019.111304.

[58] F. M. Göttsche and G. C. Hulley, "Validation of six satellite-retrieved land surface emissivity products over two land cover types in a hyper-arid region," *Remote Sens. Environ.*, vol. 124, pp. 149–158, Sep. 2012, doi: 10.1016/j.rse.2012.05.010.

[59] M. Buchhorn et al., "Copernicus global land service: Land cover 100m: Collection 3: Epoch 2019: Globe," Sep. 2020, doi: 10.5281/zenodo.3939050.

[60] S. B. Duan, Z. L. Li, N. Wang, H. Wu, and B. H. Tang, "Evaluation of six land-surface diurnal temperature cycle models using clear-sky in situ and satellite data," *Remote Sens. Environ.*, vol. 124, pp. 15–25, Sep. 2012, doi: 10.1016/j.rse.2012.04.016.

[61] J. Ma et al., "An atmospheric influence correction method for longwave radiation-based in-situ land surface temperature," *Remote Sens. Environ.*, vol. 293, 2023, Art. no. 113611, doi: 10.1016/j.rse.2023.113611.

[62] J. Gomis-Cebolla, J. C. Jimenez, and J. A. Sobrino, "LST retrieval algorithm adapted to the Amazon evergreen forests using MODIS data," *Remote Sens. Environ.*, vol. 204, pp. 401–411, 2018, doi: 10.1016/j.rse.2017.10.015.

[63] H. Li et al., "Comparison of the MuSyQ and MODIS collection 6 land surface temperature products over barren surfaces in the Heihe River Basin, China," *IEEE Trans. Geosci. Remote Sens.*, vol. 57, no. 10, pp. 8081–8094, Oct. 2019, doi: 10.1109/tgrs.2019.2918259.

[64] R. Li et al., "Land surface temperature retrieval from sentinel-3A SLSTR data: Comparison among split-window, dual-window, three-channel, and dual-angle algorithms," *IEEE Trans. Geosci. Remote Sens.*, vol. 61, Jun. 2023, Art. no. 5003114, doi: 10.1109/tgrs.2023.3288584.

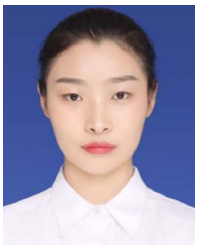

Yuting Qi received the B.S. degree in surveying and mapping engineering from Anhui Agricultural University, Hefei, China, in 2021. She is currently working toward the Ph.D. degree in geophysics with the School of Earth and Space Sciences, University of Science and Technology of China, Hefei, China.

Her research interests include algorithms for retrieval of land surface temperature over the Tibetan plateau and construction of all-sky land surface characteristics.

Lei Zhong received the B.S. degree in geographic science from Anhui Normal University, Wuhu, China, in 2001 and M.S. degree in remote sensing and geographic information systems from Anhui Normal University, Wuhu, China, in 2004, and the Ph.D. degree in natural geography from the Institute of Tibetan Plateau Research, Chinese Academy of Sciences, Beijing, China, in 2008.

He is currently a Professor with the School of Earth and Space Sciences, University of Science and Technology of China, Hefei, China. His research interests mainly focus on energy and water cycle processes between land surface and atmosphere, mainly including but not limited to energy and water cycle, land–atmosphere interaction, hydrometorology, atmospheric boundary layer process, application of remote sensing, etc.

Yaoming Ma received the B.S. degree in meteorology from Lanzhou University, Lanzhou, China, in 1987, the M.S. degree in atmospheric physics from the Lanzhou Institute of Plateau Atmospheric Physics, Chinese Academy of Sciences, Lanzhou, China, in 1995, the Ph.D. degree in atmospheric physics from National Okayama University, Okayama, Japan, in 2001, and the Ph.D. degree in environmental science from Wageningen University, Wageningen, The Netherlands, in 2006.

He is currently a Researcher with the Institute of Tibetan Plateau Research, Chinese Academy of Sciences, Beijing, China. His research interests mainly focus on atmospheric boundary layer observation and application of satellite remote sensing.

Yunfei Fu received the B.S. degree in synoptic dynamics from the Meteorology Institute of the PLA Air Force, China, in 1983, the M.S. degree in atmospheric physics and atmospheric environment from the School of Earth and Space Sciences, University of Science and Technology of China, Hefei, China, in 1990, and the Ph.D. degree in synoptic dynamics from the Institute of Atmospheric Physics, Chinese Academy of Sciences, Beijing, China, in 1993.

He is currently a Professor with the School of Earth and Space Sciences, University of Science and Technology of China. His research interests mainly focus on physical parameter retrieval of aerosol, cloud, precipitation, etc.

Zixin Wang received the B.S. degree in atmospheric science in 2021 from the School of Earth and Space Sciences, University of Science and Technology of China, Hefei, China, where she is currently working toward the Ph.D. degree in geophysics.

Her research interests focus on land surface process model and the interaction between lakes and atmosphere over the Tibetan plateau.

Peizhen Li received the B.S. degree in atmospheric science from the Chengdu University of Information Technology, Chengdu, China, in 2019. He is currently working toward the Ph.D. degree in geophysics with the School of Earth and Space Sciences, University of Science and Technology of China, Hefei, China.

His research interests focus on the estimation of all-sky shortwave radiation over the Tibetan plateau.